
Minimally distorted Adversarial Examples with a Fast Adaptive Boundary Attack

Francesco Croce
University of Tübingen

Matthias Hein
University of Tübingen

Abstract

The evaluation of robustness against adversarial manipulation of neural networks-based classifiers is mainly tested with empirical attacks as the methods for the exact computation, even when available, do not scale to large networks. We propose in this paper a new white-box adversarial attack wrt the l_p -norms for $p \in \{1, 2, \infty\}$ aiming at finding the minimal perturbation necessary to change the class of a given input. It has an intuitive geometric meaning, yields high quality results already with one restart, minimizes the size of the perturbation, so that the robust accuracy can be evaluated at all possible thresholds with a single run, and comes with almost no free parameters except number of iterations and restarts. It achieves better or similar robust test accuracy compared to state-of-the-art attacks which are partially specialized to one l_p -norm.

1 Introduction

The finding of the vulnerability of neural networks-based classifiers to adversarial examples, that is small perturbations of the input able to modify the decision of the models, started a fast development of a variety of attack algorithms. The high effectiveness of adversarial attacks reveals the fragility of these networks which questions their safe and reliable use in the real world, especially in safety critical applications. Many defenses have been proposed to fix this issue [10, 31, 23, 13, 2, 17], but with limited success, as new more powerful attacks showed [5, 1, 20]. In order to trust the decision of a given model, it is necessary to evaluate the exact adversarial robustness. Although this is possible for ReLU networks [14, 26], these techniques do not scale to commonly used large networks. Thus, the only way to derive bounds on the true robustness is by approximately solving the minimal adversarial perturbation problem through adversarial attacks.

One can distinguish attacks into black-box attacks [21, 3, 25], where one is only allowed to query the classifier and has no access to the network itself, and white-box attacks, where one has full control over the network, according to the attack model used to create adversarial examples (typically some l_p -norm, but others have become popular as well [4, 9, 29]), whether they aim at the minimal adversarial perturbation [6, 7, 8] or rather any perturbation below a threshold [16, 17, 32], if they have lower [19, 18] or higher [6, 8] computational cost. Moreover, it is clear that due to the non-convexity of the minimal adversarial perturbation problem there exists no universally best attack (apart from the exact methods), since this depends on runtime constraints, networks architecture, dataset etc. However, our goal is to have an attack which performs well under a broad spectrum of conditions with minimal amount of hyperparameter tuning.

In this paper we propose a new white-box attacking scheme which performs comparably or better than established attacks and has the following features: first, it tries to produce adversarial samples with *minimal distortion* compared to the original point, measured wrt the l_p -norms with $p \in \{1, 2, \infty\}$. Compared to the quite popular PGD-attack [16, 17] this has

the clear advantage that the method does not need to be restarted for every new threshold ϵ if one wants to evaluate the success rate of the attack with adversarial perturbations constrained to be in $\{\delta \in \mathbb{R}^d \mid \|\delta\|_p \leq \epsilon\}$, and thus is particularly suitable in order to have a more complete picture on the robustness of a neural network for several thresholds ϵ . Second, it achieves *fast* good quality in terms of average distortion resp. robust accuracy compared to the PGD-attack and other fast attacks. At the same time we show that increasing the number of restarts keeps improving the results and makes it competitive with the strongest available attacks. Third, although it comes with a few parameters, these generalize across datasets, architectures and norms considered, so that we have an almost *off-the-shelf method* for which it is sufficient to specify the number of iterations and restarts. Most importantly compared to PGD and other methods there is no stepsize parameter which potentially has to be carefully adapted to every new network.

2 FAB: a Fast Adaptive Boundary Attack

We first introduce minimal adversarial samples before we recall the definition and properties of the projection wrt the l_p -norms of a point on the intersection of a hyperplane and box constraints, as they are an essential part of our attack. Then we present our FAB-attack algorithm to generate minimal adversarial examples.

2.1 Minimal adversarial examples

Let $f : \mathbb{R}^d \rightarrow \mathbb{R}^K$ be a classifier which assigns every input $x \in \mathbb{R}^d$ (with d the dimension of the input space) to one of the K classes according to $\arg \max_{r=1, \dots, K} f_r(x)$. In many scenarios the input of f has to satisfy a specific set of constraints C , e.g. images are represented as elements of $[0, 1]^d$. Then, given a point $x \in \mathbb{R}^d$ with true class c , we define the *minimal adversarial example* for x wrt the l_p -norm as

$$\delta_{\min,p} = \arg \min_{\delta \in \mathbb{R}^d} \|\delta\|_p, \quad \text{s.th.} \quad \max_{l \neq c} f_l(x + \delta) \geq f_c(x + \delta), \quad x + \delta \in C. \quad (1)$$

The optimization problem (1) is non-convex and NP-hard for non-trivial classifiers [14] and although for some classes of networks it can be formulated as a mixed-integer program [26] the computational cost of solving it is prohibitive for large, normally trained networks. Thus, $\delta_{\min,p}$ is usually approximated by an *attack algorithm*, which can be seen as heuristic to solve (1). We will see in the experiments that it can happen that current attacks drastically overestimate $\delta_{\min,p}$ and thus seemingly robust networks are actually not robust at all.

2.2 Projection on a hyperplane with box constraints

Let $w \in \mathbb{R}^d$ and $b \in \mathbb{R}$ be the normal vector and the offset defining the hyperplane $\pi : \langle w, x \rangle + b = 0$. Let $x \in \mathbb{R}^d$, we denote by the *box constrained projection* wrt the l_p -norm of x on π (projection onto the intersection of the box $C = \{u \in \mathbb{R}^d : l_i \leq u \leq u_i\}$ and the hyperplane π) the following minimization problem:

$$z^* = \arg \min_{z \in \mathbb{R}^d} \|z - x\|_p \quad \text{s.th.} \quad \langle w, z \rangle + b = 0, \quad l_i \leq z_i \leq u_i, \quad i = 1, \dots, d, \quad (2)$$

where $l_i, u_i \in \mathbb{R}$ are lower and upper bounds on each component of z . For $p \geq 1$ the optimization problem (2) is convex. Moreover, [12] proved that for $p \in \{1, 2, \infty\}$ the solution can be obtained in $\mathcal{O}(d \log d)$ time, that is the complexity of sorting a vector of d elements, as well as determining that it has no solution. This can be seen by going to the dual problem of (2) which reduces to a one-dimensional convex optimization problem.

Since this projection is part of our iterative scheme to generate adversarial examples, we need to handle specifically the case of (2) being infeasible. In this case, defining $\rho = \text{sign}(\langle w, x \rangle + b)$, we instead compute

$$z' = \arg \min_{z \in \mathbb{R}^d} \rho(\langle w, z \rangle + b) \quad \text{s.th.} \quad l_i \leq z_i \leq u_i, \quad i = 1, \dots, d, \quad (3)$$

whose solution is given componentwise, for every $i = 1, \dots, d$, by $z_i = \begin{cases} l_i & \text{if } \rho w_i > 0, \\ u_i & \text{if } \rho w_i < 0, \\ x_i & \text{if } w_i = 0 \end{cases}$.

Assuming that the point x satisfies the box constraints (as it will be in our algorithm), this is equivalent to identifying the corner of the d -dimensional box defined by the componentwise constraints on z closest to the hyperplane π . Notice that if (2) is infeasible then the objective function of (3) stays positive and the points x and z are strictly contained in the same of the two halfspaces divided by π . Finally, we define the operator

$$\text{proj}_p : (x, \pi, C) \mapsto \begin{cases} z^* & \text{if Problem (2) is feasible} \\ z' & \text{else} \end{cases}, \quad (4)$$

which basically yields the point which gets as close as possible to the hyperplane π without violating the box constraints.

2.3 FAB Attack

We introduce now our algorithm¹ to produce minimally distorted adversarial examples, wrt any l_p -norm for $p \in \{1, 2, \infty\}$, for a given point x_{orig} initially correctly classified by f as class c . The high-level idea is that we use the linearization of the classifier at the current iterate $x^{(i)}$ and compute the box-constrained projections of $x^{(i)}$ respectively x_{orig} onto the approximated decision hyperplane and take a convex combinations of these projections depending on the distance of $x^{(i)}$ and x_{orig} to the decision hyperplane, followed by some extrapolation step. We explain below the geometric motivation behind these steps. The attack closest in spirit is DeepFool [19] which is known to be very fast but suffers from low quality. The main reason is that DeepFool is just trying to find the decision boundary quickly but has no incentive to provide a solution close to x_{orig} . Our scheme resolves this main problem and, together with the exact projection we use, leads to a principled way to track the decision boundary (that is the surface where the decision of f changes) *close to* x_{orig} .

If f was a linear classifier then the closest point to $x^{(i)}$ on the decision hyperplane could be found in closed form. Although neural networks are highly non-linear, so called ReLU networks (neural networks which use ReLU as activation function, and possibly max- and average pooling) are piecewise affine functions and thus locally a linearization of the network is an exact description of the classifier. Let $l \neq c$, then the decision boundary between classes l and c can be locally approximated using a first order Taylor expansion at $x^{(i)}$ by the hyperplane

$$\pi_l(z) : f_l(x^{(i)}) - f_c(x^{(i)}) + \left\langle \nabla f_l(x^{(i)}) - \nabla f_c(x^{(i)}), z - x^{(i)} \right\rangle = 0. \quad (5)$$

Moreover the l_p -distance $d_p(\pi, x^{(i)})$ of $x^{(i)}$ to π_l is given by

$$d_p(\pi_l, x^{(i)}) = \frac{|f_l(x^{(i)}) - f_c(x^{(i)})|}{\|\nabla f_l(x^{(i)}) - \nabla f_c(x^{(i)})\|_q}, \quad \text{with } \frac{1}{p} + \frac{1}{q} = 1. \quad (6)$$

Note that if $d_p(\pi_l, x^{(i)}) = 0$ then $x^{(i)}$ belongs to the true decision boundary. Moreover, if the local linear approximation of the network is correct then the class s with the decision hyperplane closest to the point $x^{(i)}$ can be computed as

$$s = \arg \min_{l \neq c} \frac{|f_l(x^{(i)}) - f_c(x^{(i)})|}{\|\nabla f_l(x^{(i)}) - \nabla f_c(x^{(i)})\|_q}. \quad (7)$$

Thus, given that the approximation holds in some large enough neighborhood, the projection $\text{proj}_p(x^{(i)}, \pi_s, C)$ of $x^{(i)}$ onto π_s lies on the decision boundary (unless Problem (2) is infeasible).

¹<https://github.com/fra31/fab-attack>

Biased gradient step: The iterative algorithm, $x^{(i+1)} = \text{proj}_p(x^{(i)}, \pi_s, C)$, would be similar to DeepFool [19] with the difference that our projection operator is exact whereas they project onto the hyperplane and then do clipping in order to satisfy the box constraints. However, the problem with this scheme is that there is no bias towards the original target point x_{orig} after the algorithm has been started. Thus it goes typically further than necessary to find a point on the decision boundary as basically the algorithm just tracks the decision boundary without aiming at the minimal adversarial perturbation. Thus we consider additionally $\text{proj}_p(x_{\text{orig}}, \pi_s, C)$ and use instead the iterative step, with $x^{(0)} = x_{\text{orig}}$, defined as

$$x^{(i+1)} = (1 - \alpha) \cdot \text{proj}_p(x^{(i)}, \pi_s, C) + \alpha \cdot \text{proj}_p(x_{\text{orig}}, \pi_s, C), \quad (8)$$

which biases the step towards x_{orig} (see Figure 1). Note that this is a convex combination of points on π_s both contained in C and thus also their convex combination lies on π_s and is contained in C . The next question is how to choose α . As we are aiming at a scheme with minimal amount of parameters, we want to have an automatic selection of α based on the available geometric quantities. Let

$$\delta^{(i)} = \text{proj}_p(x^{(i)}, \pi_s, C) - x^{(i)} \quad \text{and} \quad \delta_{\text{orig}}^{(i)} = \text{proj}_p(x_{\text{orig}}, \pi_s, C) - x_{\text{orig}}.$$

Note that $\|\delta^{(i)}\|_p$ and $\|\delta_{\text{orig}}^{(i)}\|_p$ are the distances of $x^{(i)}$ and x_{orig} to π_s (inside C). We propose to use for the parameter α the relative magnitude of these two distances, that is

$$\alpha = \min \left\{ \frac{\|\delta^{(i)}\|_p}{\|\delta^{(i)}\|_p + \|\delta_{\text{orig}}^{(i)}\|_p}, \alpha_{\text{max}} \right\} \in [0, 1]. \quad (9)$$

The motivation for doing so is that if $x^{(i)}$ is close to the decision boundary, then we should stay close to this point (note that π_s is the approximation of f computed at $x^{(i)}$ and thus it is valid in a small neighborhood of $x^{(i)}$, whereas x_{orig} is farther away). On the other hand we want to have the bias towards x_{orig} in order not to go too far away from x_{orig} . This is why α depends on the distances of $x^{(i)}$ and x_{orig} to π_s but we limit with α_{max} the amount of the step we go towards x_{orig} as the approximation at $x^{(i)}$ of f is not likely to be valid around x_{orig} . Finally, we use a small extrapolation step as we noted empirically, similarly to [19], that this helps to cross faster the decision boundary and get an adversarial sample. This leads to the final scheme:

$$x^{(i+1)} = \text{proj}_C \left((1 - \alpha)(x^{(i)} + \eta\delta^{(i)}) + \alpha(x_{\text{orig}} + \eta\delta_{\text{orig}}^{(i)}) \right), \quad (10)$$

where α is chosen as in (9), $\eta \geq 1$ and proj_C is just the projection onto the box which can be done by clipping. In Figure 1 we visualize the scheme: in black one can see the hyperplane π_s and the vectors $\delta_{\text{orig}}^{(i)}$ and $\delta^{(i)}$, in blue the step we would make going to the decision boundary with the DeepFool variant, while in red the actual step we have in our method. The green vector represents instead the bias towards the original point we introduce. On the left of Figure 1 we use $\eta = 1$, while on the right we use overshooting $\eta > 1$.

Interpretation of $\text{proj}_p(x_{\text{orig}}, \pi_s, C)$: The projection of the target point onto the intersection of π_s and C is defined as

$$\arg \min_{z \in \mathbb{R}^d} \|z - x_{\text{orig}}\|_p \quad \text{s.th.} \quad \langle w, z \rangle + b = 0, \quad l_i \leq z_i \leq u_i,$$

Note that replacing z by $x^{(i)} + \delta$ we can rewrite this as

$$\arg \min_{\delta \in \mathbb{R}^d} \left\| x^{(i)} + \delta - x_{\text{orig}} \right\|_p \quad \text{s.th.} \quad \langle w, x + \delta \rangle + b = 0, \quad l_i \leq x_i + \delta_i \leq u_i,$$

This can be interpreted as the minimization of the distance of the next iterate $x^{(i)} + \delta$ to the target point x_{orig} so that $x^{(i)} + \delta$ lies on the intersection of the (approximate) decision hyperplane and the box C . This point of view on the projection $\text{proj}_p(x_{\text{orig}}, \pi_s, C)$ again justifies using a convex combination of the two projections in our iterative scheme in (10).

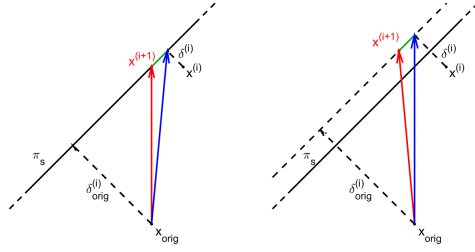


Figure 1: Visualization of FAB-attack scheme, with on the left the case $\eta = 1$, on the right $\eta > 1$. In blue we represent the next iterate $x^{(i+1)}$ one would get without any bias toward the original point x_{orig} , in green the effect of the bias we introduce and in red the $x^{(i+1)}$ obtained with our scheme in (10). We see that our algorithm tends to stay closer to the original point compared to the one with an unbiased gradient step.

Backward step: The described scheme finds in a few iterations adversarial perturbations. However, we are interested in minimizing their norms. Thus, once we have a new point $x^{(i+1)}$, we check whether it is assigned by f to a class different from c . In this case, we apply

$$x^{(i+1)} = (1 - \beta)x_{\text{orig}} + \beta x^{(i+1)}, \quad \beta \in (0, 1), \quad (11)$$

that is we go back towards x_{orig} on the segment $[x^{(i+1)}, x_{\text{orig}}]$, effectively starting again the algorithm at a point which is quite close to the decision boundary. In this way, due to the bias of the method towards x_{orig} we successively find adversarial perturbations of smaller norm, meaning that the algorithm *tracks* the decision boundary while getting closer to x_{orig} .

Final search: Our scheme finds points close to the decision boundary but often they are slightly off as the linear approximation is not exact and we apply the extrapolation step with $\eta > 1$. Thus, after finishing N_{iter} iterations of our algorithmic scheme, we perform a last, fast step to further improve the quality of the adversarial examples. Let x_{out} be the closest point to x_{orig} classified differently from c , say $s \neq c$, found with the iterative scheme. It holds that $f_s(x_{\text{out}}) - f_c(x_{\text{out}}) > 0$ and $f_s(x_{\text{orig}}) - f_c(x_{\text{orig}}) < 0$. This means that, assuming f continuous, there exists a point x^* on the segment $[x_{\text{out}}, x_{\text{orig}}]$ such that $f_s(x^*) - f_c(x^*) = 0$ and $\|x^* - x_{\text{orig}}\|_p < \|x_{\text{out}} - x_{\text{orig}}\|_p$. If f is linear

$$x^* = x_{\text{out}} - \frac{f_s(x_{\text{out}}) - f_c(x_{\text{out}})}{f_s(x_{\text{out}}) - f_c(x_{\text{out}}) + f_s(x_{\text{orig}}) - f_c(x_{\text{orig}})}(x_{\text{out}} - x_{\text{orig}}). \quad (12)$$

Since f is typically non-linear, but close to linear, we compute iteratively for a few steps

$$x_{\text{temp}} = x_{\text{out}} - \frac{f_s(x_{\text{out}}) - f_c(x_{\text{out}})}{f_s(x_{\text{out}}) - f_c(x_{\text{out}}) + f_s(x_{\text{orig}}) - f_c(x_{\text{orig}})}(x_{\text{out}} - x_{\text{orig}}), \quad (13)$$

each time replacing in (13) x_{out} with x_{temp} if $f_s(x_{\text{temp}}) - f_c(x_{\text{temp}}) > 0$ or x_{orig} with x_{temp} if instead $f_s(x_{\text{temp}}) - f_c(x_{\text{temp}}) < 0$. With this kind of modified binary search one can find a better adversarial sample with the cost of a few forward passes of the network.

Random restarts: So far all the steps are deterministic. However, in order to improve the results, we introduce the option of random restarts, that is $x^{(0)}$ is randomly sampled in proximity of x_{orig} instead of being x_{orig} itself. Most attacks benefit from random restarts [17, 32], especially when attacking models protected by gradient-masking defenses [20], as they allow a wider exploration of the input space. In particular, we choose to sample from the l_p -sphere centered in the original point with radius half the l_p -norm of the current best adversarial perturbation (or a given threshold if no adversarial example has been found yet).

Computational cost: Our attack, summarized in Algorithm 1, consists of two main operations: the computation of f and its gradient and solving the projection problem (2). In particular, we perform, for each iteration, a forward and a backward pass of the network in the gradient step and a forward pass in the backward step. Regarding the projection, we mentioned that its complexity is $\mathcal{O}(d \log d)$ for an input of dimension d [12] and it can

Algorithm 1: FAB-attack

Input : x_{orig} original point, c original class, $N_{\text{restarts}}, N_{\text{iter}}, \alpha_{\text{max}}, \beta, \eta, \epsilon, p$ **Output** : x_{out} adversarial example

```
1  $u \leftarrow +\infty$ 
2 for  $j = 1, \dots, N_{\text{restarts}}$  do
3   if  $j = 1$  then  $x^{(0)} \leftarrow x_{\text{orig}}$ ;
4   else  $x^{(0)} \leftarrow$  randomly sampled s.th.  $\|x^{(0)} - x_{\text{orig}}\|_p = \min\{u, \epsilon\}/2$ ;
5   for  $i = 0, \dots, N_{\text{iter}} - 1$  do
6      $s \leftarrow \arg \min_{l \neq c} \frac{|f_l(x^{(i)}) - f_c(x^{(i)})|}{\|\nabla f_l(x^{(i)}) - \nabla f_c(x^{(i)})\|_q}$ 
7      $\delta^{(i)} \leftarrow \text{proj}_p(x^{(i)}, \pi_s, C)$ 
8      $\delta_{\text{orig}}^{(i)} \leftarrow \text{proj}_p(x_{\text{orig}}, \pi_s, C)$ 
9     compute  $\alpha$  as in Equation (9)
10     $x^{(i+1)} \leftarrow \text{proj}_C\left((1 - \alpha)(x^{(i)} + \eta\delta^{(i)}) + \alpha(x_{\text{orig}} + \eta\delta_{\text{orig}}^{(i)})\right)$ 
11    if  $x^{(i+1)}$  is not classified in  $c$  then
12      if  $\|x^{(i+1)} - x_{\text{orig}}\|_p < u$  then
13         $x_{\text{out}} \leftarrow x^{(i+1)}$ 
14         $u \leftarrow \|x^{(i+1)} - x_{\text{orig}}\|_p$ 
15      end
16       $x^{(i+1)} \leftarrow (1 - \beta)x_{\text{orig}} + \beta x^{(i+1)}$ 
17    end
18  end
19 end
20 perform 3 steps of final search on  $x_{\text{out}}$  as in (13)
```

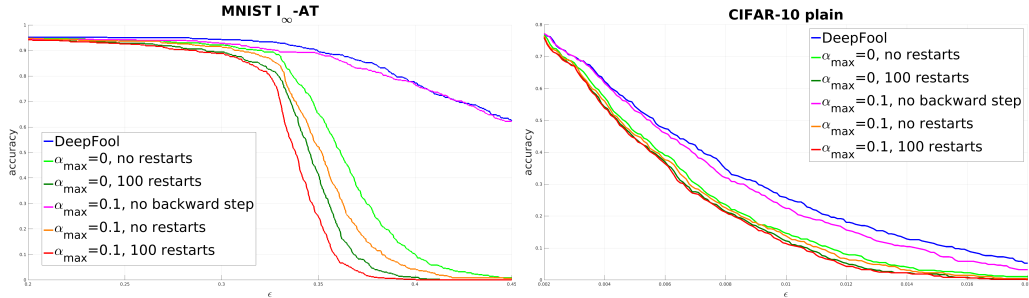


Figure 2: Ablation study to DeepFool [19] for l_∞ -attacks. The introduction of the convex combination ($\alpha_{\text{max}} = 0.1$, no backward step) already improves over DeepFool. Moreover, if one does our full approach, the case $\alpha_{\text{max}} = 0$ (can be seen as an improved iterative DeepFool) is worse than $\alpha_{\text{max}} = 0.1$. In the plots we show the robust accuracy as a function of the threshold ϵ under the different attacks on the l_∞ -AT model on MNIST (left) and the *plain* model on CIFAR-10 (right).

be efficiently implemented so that it runs in batches on the GPU. Moreover, it does not depend on the architecture of the network, meaning that, except for shallow models, its cost is by far smaller than the passes through the network. Overall, we can approximate the computational cost of our algorithm by the total number of calls of the classifier

$$N_{\text{iter}} \times N_{\text{restarts}} \times (2 \times \text{forward passes} + 1 \times \text{backward pass}). \quad (14)$$

One has to add the forward passes for the final search, which we set in the experiments to 3, that however happens just once.

2.4 Comparison to DeepFool [19]

The idea of exploiting the first order local approximation of the decision boundary is not novel but the basis of one of the first white-box adversarial attacks, DeepFool [19]. While

DeepFool and our FAB-attack share the strategy of using a linear approximation of the classifier and doing steps based on projecting on the decision hyperplanes, we want to point out many key differences: first, [19] do not solve the projection problem (2) exactly but rather its simpler version without box constraints and clipping afterwards. Second, their gradient step does not have any bias towards the original point, that is they have always $\alpha = 0$ in (10). Third, DeepFool does not have any backward step, final search or restart, as it stops as soon as it finds a point with different classification (to be fair its main goal is to provide quickly an adversarial perturbation of average quality).

We perform an ablation study of the differences to DeepFool in Figure 2, where we show the curves of the robust accuracy as a function of the threshold ϵ (we define properly the robust accuracy in Section 3 but in the plots lower is better), on two models, for various l_∞ -attacks. In particular, we present the results of DeepFool (blue) and FAB-attack with the following variations: $\alpha_{\max} = 0.1$ and no backward step (magenta), $\alpha_{\max} = 0$ (that is no bias in the gradient step) and no restarts (light green), $\alpha_{\max} = 0$ and 100 restarts (dark green), $\alpha_{\max} = 0.1$ and no restarts (orange) and $\alpha_{\max} = 0.1$ and 100 restarts, that is FAB-attack, (red). We can see how every addition we make to the original scheme of DeepFool contributes to the significantly improved performance of FAB-attack when compared to the original DeepFool.

3 Experiments

We compare our FAB-attack to other state-of-the-art attacks on MNIST, CIFAR-10 [15] and Restricted ImageNet [28]. For each dataset we consider a naturally trained model (*plain*) and two adversarially trained ones as in [17], one to achieve robustness wrt the l_∞ -norm (l_∞ -AT) and the other wrt the l_2 -norm (l_2 -AT). In particular the *plain* and l_∞ -AT models on MNIST are those available at https://github.com/MadryLab/mnist_challenge and consist of two convolutional and two fully-connected layers. The architecture of the CIFAR-10 models, which can be found at <https://github.com/fra31/fab-attack>, has 8 convolutional layers (with number of filters increasing from 96 to 384) and 2 dense layers, while on Restricted ImageNet we use the models (ResNet-50 [11]) from [28] and available at <https://github.com/MadryLab/robust-features-code>.

We test the robustness of each model wrt the l_∞ -, l_2 - and l_1 -norm attack models and compare the performances of FAB-attack to those of attacks representing the state-of-the-art in each norm: DeepFool (DF) [19], Carlini-Wagner l_2 -attack (CW) [6], Linear Region l_2 -Attack (LRA) [8], Projected Gradient Descent on the cross-entropy function (PGD) [16, 17, 27], Distributionally Adversarial Attack (DAA), [32], SparseFool [18], Elastic-net Attack (EAD) [7]. We use DF as implemented in [24], CW and EAD as in [22], with 10000 and 1000 iterations respectively, and EAD with the l_1 decision rule and $\beta = 0.05$ to achieve the l_1 -minimally distorted adversarial examples. We use DAA and LRA with the code from the original papers, while we reimplemented SparseFool and PGD.

In order to have a more complete overview of the behaviour of the different algorithms we consider multiple combinations of amounts of random restarts and iterations. In particular, on MNIST and CIFAR-10, for PGD wrt l_∞ and l_2 we report the results with 40 iterations and 1, 100, 500 restarts, for PGD wrt l_1 100 iterations and 1, 50, 100 restarts. For DAA we use 1 and 50 restarts, 200 iterations on MNIST and 50 iterations on CIFAR-10. Finally, for our method we report the results with 100 iterations and 1, 10, 100 random restarts. For the experiments on Restricted ImageNet we could not use LRA since it hardly scales to such models and CW and EAD for compatibility issues between the implementation of the attacks and that of the models. For PGD wrt l_∞ and l_2 we set 40 iterations for each restart (1 and 50 reported), while for PGD wrt l_1 100 iterations (1 and 20 restarts reported). For DAA we use 50 iterations and 10 restarts. Moreover, FAB-attack is given 100 iterations for l_∞ and l_2 , 300 for l_1 (in general we notice that l_1 -attacks require more iterations), 1 and 10 restarts.

In Tables 1 to 9 we report the effectiveness of the attacks evaluating upper bounds on the *robust accuracy*, that is, for a fixed threshold ϵ , the percentage of test points for which the attack could not find an adversarial perturbation with norm smaller than ϵ . Please note that PGD and DAA cannot evaluate more than one ϵ at the same time, so that they need to be rerun multiple times, unlike the other methods for which a single run is sufficient to obtain

the full statistics.

We observe that, while in general it is not possible to determine a universal best method and all of them present at least one case where they are far from the optimal performance, FAB-attack is able to compete and even outperform in most of the scenarios algorithms specialized in a specific norm. In particular, on MNIST l_∞ -AT we see that DAA is the best one wrt l_∞ , our method is not far, at least with 100 restarts, and at the same time achieves the lowest (lower is better) values for l_2 , where with multiple restarts it competes with the very expensive LRA, and for l_1 FAB-attack is notably better than EAD. On the other hand on CIFAR-10 l_2 -AT FAB-attack, already with a single restart, outperforms the competing methods in l_∞ , is comparable to CW and LRA in l_2 , and slightly worse with 1 and 10 restarts but better with 100 restarts than EAD in l_1 . On Restricted ImageNet, for l_∞ and l_2 there is a slight prevalence of PGD or DAA, for l_1 FAB-attack consistently outperforms the competing methods.

Runtime comparison: While a comparison of the computational cost of the various methods is not straightforward we tried our best to provide a fair budget to each of them. First, DeepFool and SparseFool are definitely significantly faster than the others as their primary goal is to succeed as soon as possible in finding adversarial examples, without emphasis on minimizing their norms. Second, CW and LRA are rather expensive attacks as noted in [8]. Third, we can roughly compare the runtime of EAD to that of FAB-attack with 25 restarts and 100 iterations. For DAA, we can say that on MNIST, using the same parameters as in [32], the runtime of DAA-50 is comparable to that of FAB-attack with 100 restarts and 100 iterations, with the remarkable difference that DAA has to be restarted for every threshold ϵ . Finally, each iteration of PGD consists in one forward and one backward pass of the network. If we do not consider the additional but negligible cost of the projection on the decision hyperplane of our method, we can compare PGD and FAB-attack wrt the number of forward and backward passes of the model performed in total (see (14)). From this point of view PGD-100 used for l_∞ and l_2 in the tables, with 40 iterations, requires, for every ϵ , roughly the same number of forward/backward passes as FAB-attack with 27 restarts and 100 iterations.

In summary, our attack is based on a solid geometric motivation, very competitive both in quality and in runtime compared to state-of-the-art attacks and at the same time flexible as it can be used for all p -norms in $p \in \{1, 2, \infty\}$ which is not the case for most other methods.

3.1 Testing standard benchmarks

In order to further validate the effectiveness of our FAB-attack, we test it on models obtained via the state-of-the-art in training robust models, that is [17] and [30]. Since here the main focus is on producing the strongest adversarial examples rather than having an efficient attack, we introduce for these experiments a so-called *targeted* version of FAB-attack. Explicitly, at step 6 of Algorithm 1, instead of choosing the hyperplane on which we project as the closest one to the current iterate, we always take the one separating the original class from a specified target class t , that is we fix $s = t$. Note that this is not actually a targeted attack since we do not ensure that the final output x_{out} is classified as t , although it is likely to happen. However, in this way we allow an exploration of the input space even in directions which are not usually considered by the standard algorithm, at the price of a higher computational cost as we run the attack for all the $K - 1$ possible values of t (all the alternative classes).

With this additional option, we could improve the results of the CIFAR-10 challenge at https://github.com/MadryLab/cifar10_challenge, decreasing the robust accuracy of the proposed model to 44.51% at thresholds $\epsilon = 8/255$ in l_∞ -norm, that is 0.2% lower than the best result so far (we performed 10 restarts of FAB-attack with 150 iterations, achieving already 45.28%, plus 5 restarts of the targeted version).

Moreover, we tested a further modification of our algorithm: instead of performing the line search described in Section 2 only once as the last step of the procedure (called *final search* in Section 2), we apply the line search every time the attack finds a new adversarial example. In this way one has intermediate solutions which lie closer to the decision boundary than in the usual approach, at the cost of a higher runtime. In Tables 10 and 11 in Section A of the

Table 1: Comparison of l_∞ -, l_2 - and l_1 -attacks on an l_∞ -robust model on MNIST. We report the accuracy on the test set if the attack is allowed to perturb the test points of ϵ in l_p -distance. The statistics are computed on the first 1000 points on the test set for l_∞ and l_1 , on 500 points for l_2 .

Robust accuracy of MNIST l_∞ -robust model										
metric	ϵ	DF	DAA-1	DAA-50	PGD-1	PGD-100	PGD-500	FAB-1	FAB-10	FAB-100
l_∞	.2	95.2	94.6	93.7	94.9	93.8	93.8	94.7	94.3	93.7
	0.25	94.7	92.7	91.1	93.9	91.5	91.3	93.3	91.9	91.6
	0.3	93.9	89.5	87.2	92.0	88.0	87.5	91.2	89.3	88.4
	0.325	92.5	72.1	64.2	82.5	72.4	70.9	86.6	83.3	81.3
	0.35	89.8	19.7	11.7	43.4	20.4	17.5	51.3	31.3	23.0
		CW	DF	LRA	PGD-1	PGD-100	PGD-500	FAB-1	FAB-10	FAB-100
l_2	1	88.8	94.6	73.6	92.6	89.8	89.4	83.6	70.8	64.6
	1.5	77.6	93.0	25.8	87.8	80.6	77.8	46.2	20.8	12.4
	2	64.4	91.6	3.2	81.0	67.2	64.0	15.6	2.2	0.2
	2.5	53.8	89.6	0.4	73.0	46.4	38.2	3.8	0.0	0.0
	3	46.8	84.6	0.0	67.6	23.0	14.6	1.4	0.0	0.0
		SparseFool	EAD	PGD-1	PGD-50	PGD-100	FAB-1	FAB-10	FAB-100	
l_1	2.5		96.8	92.2	94.1	93.9	93.6	83.1	66.1	54.2
	5		96.5	76.0	91.0	89.9	88.0	59.2	26.2	14.5
	7.5		96.4	49.5	86.2	82.8	79.3	48.6	13.3	5.1
	10		96.4	27.4	80.1	73.3	66.8	45.0	9.6	2.4
	12.5		96.4	14.6	74.2	62.0	52.7	43.1	8.0	1.1

Appendix we repeat the experiments of Tables 1 to 9, using the highest number of restarts, with this modified version, showing that in general there is no large improvement. However, in the case of the model of the CIFAR-10 challenge, we could further decrease the robust accuracy to 44.39% with 10 restarts of the untargeted version (which lead to 45.09% of robust accuracy) and 5 restarts of the targeted one (150 iterations) using this modification.

Furthermore, we attacked the models on MNIST and CIFAR-10 presented in [30] and available at <https://github.com/yaodongyu/TRADES>, which are considered more robust than those obtained by the standard adversarial training of [17]. For MNIST, the lowest robust accuracy wrt l_∞ at $\epsilon = 0.3$ so far achieved was 95.60%, while FAB-attack is able to reduce it to 93.33% (100 restarts in the untargeted scenario plus 10 restarts of the targeted version, both with 1000 iterations). A cheaper version of FAB-attack, with 100 iterations, no random restarts and in the usual untargeted version, decreases accuracy to 94.94%. Similarly on CIFAR-10, our attack reduces the robust accuracy at $\epsilon = 0.031$ from 56.43% to 53.44% (5 restarts of the untargeted version plus 5 restarts of the targeted version, both with 100 iterations). Notably, already a weaker version of our untargeted attack, with 20 iterations and no restarts, reaches 54.64%, that is almost 2% better than the previous best result.

3.2 Experimental details

The models on MNIST achieve the following clean accuracy: *plain* 98.7%, l_∞ -AT 98.5%, l_2 -AT 98.6%. The models on CIFAR-10 achieve the following clean accuracy: *plain* 89.2%, l_∞ -AT 79.4%, l_2 -AT 81.2%.

For PGD wrt l_∞ we use, given a threshold ϵ , a step size of $\epsilon/10$, for PGD wrt l_2 we perform at each iteration a step in the direction of the gradient of size $\epsilon/4$, for PGD wrt l_1 we use the gradient step suggested in [27], with size $\epsilon/2$.

For FAB-attack we use the following parameters for all the cases on MNIST and CIFAR-10: $\alpha_{\max} = 0.1$, $\eta = 1.05$, $\beta = 0.9$. On Restricted ImageNet we set $\alpha_{\max} = 0.05$, $\eta = 1.05$, $\beta = 0.9$. Moreover, the value of ϵ used for sampling in the case of random restarts is chosen to be comparable to the expected size of the perturbations (for more details see Section A.1 of the Appendix).

Table 2: Comparison of l_∞ -, l_2 - and l_1 -attacks on an l_2 -robust model on MNIST. We report the accuracy in percentage of the classifier on the test set if the attack is allowed to perturb the test points of ϵ in l_p -distance. The statistics are computed on the first 1000 points on the test set for l_∞ and l_1 , on 500 points for l_2 .

Robust accuracy of MNIST l_2 -robust model										
metric	ϵ	DF	DAA-1	DAA-50	PGD-1	PGD-100	PGD-500	FAB-1	FAB-10	FAB-100
l_∞	0.05	96.7	96.4	96.3	96.4	96.4	96.3	96.6	96.4	96.4
	0.1	93.4	91.0	90.2	91.0	90.4	90.4	90.6	90.6	90.4
	0.15	86.4	74.3	72.3	75.2	72.8	72.5	73.4	72.2	71.8
	0.2	73.8	34.5	27.2	36.8	27.5	25.9	34.0	28.8	26.0
	0.25	55.1	1.5	0.9	2.9	0.9	0.9	2.2	1.0	0.8
		CW	DF	LRA	PGD-1	PGD-100	PGD-500	FAB-1	FAB-10	FAB-100
l_2	1	92.6	93.8	92.6	93.0	93.0	93.0	92.8	92.6	92.6
	1.5	84.8	87.2	83.4	84.2	83.4	83.4	83.8	83.6	83.6
	2	70.6	79.0	68.0	70.2	68.2	67.8	70.0	69.2	68.0
	2.5	46.4	67.4	41.6	47.2	39.4	38.2	46.8	42.4	38.6
	3	17.2	54.2	11.2	22.8	10.6	10.4	20.0	12.6	11.6
		SparseFool	EAD	PGD-1	PGD-50	PGD-100	FAB-1	FAB-10	FAB-100	
l_1	5		94.9	89.8	90.2	90.2	90.2	90.5	90.4	90.1
	8.75		89.1	71.2	75.6	73.7	72.9	75.4	74.0	72.6
	12.5		81.0	45.9	60.0	56.8	54.8	55.5	49.4	45.9
	16.25		72.8	20.6	46.6	40.0	35.7	33.6	24.8	20.7
	20		60.8	8.3	37.2	26.3	20.7	16.1	9.6	7.7

Table 3: Comparison of l_∞ -, l_2 - and l_1 -attacks on a naturally trained model on MNIST. We report the accuracy in percentage of the classifier on the test set if the attack is allowed to perturb the test points of ϵ in l_p -distance. The statistics are computed on the first 1000 points on the test set for l_∞ and l_1 , on 500 points for l_2 .

Robust accuracy of MNIST plain model										
metric	ϵ	DF	DAA-1	DAA-50	PGD-1	PGD-100	PGD-500	FAB-1	FAB-10	FAB-100
l_∞	0.03	93.2	91.9	91.9	92.0	91.9	91.9	93.8	93.6	93.6
	0.05	83.4	78.2	76.7	77.1	75.6	75.2	77.8	77.4	77.2
	0.07	61.5	59.8	56.3	45.0	41.8	41.5	45.2	43.4	42.8
	0.09	33.2	46.7	41.0	17.6	14.3	13.7	16.4	15.4	15.2
	0.11	13.1	34.4	26.2	4.2	2.8	2.7	3.4	2.8	2.4
		CW	DF	LRA	PGD-1	PGD-100	PGD-500	FAB-1	FAB-10	FAB-100
l_2	0.5	92.6	93.6	92.6	92.6	92.6	92.6	92.6	92.6	92.6
	1	47.4	58.6	47.4	49.6	48.2	47.6	47.2	46.8	46.8
	1.5	8.8	19.8	7.8	10.0	10.0	10.0	8.0	7.4	7.4
	2	0.6	1.8	0.2	0.6	0.6	0.6	0.2	0.2	0.2
	2.5	0.0	0.0	0.0	0.2	0.2	0.2	0.0	0.0	0.0
		SparseFool	EAD	PGD-1	PGD-50	PGD-100	FAB-1	FAB-10	FAB-100	
l_1	2		95.5	93.6	94.2	93.8	93.6	94.1	93.6	93.5
	4		88.9	76.7	80.3	77.5	76.2	80.0	76.1	75.4
	6		75.8	48.1	55.9	49.8	46.7	54.2	47.1	43.0
	8		60.3	26.6	36.6	28.5	25.2	30.9	23.9	22.8
	10		43.8	11.2	25.8	15.4	12.7	15.1	10.3	8.2

Table 4: Comparison of l_∞ -, l_2 - and l_1 -attacks on an l_2 -robust model on CIFAR-10. We report the accuracy in percentage of the classifier on the test set if the attack is allowed to perturb the test points of ϵ in l_p -distance. The statistics are computed on the first 1000 points on the test set for l_∞ and l_1 , on 500 points for l_2 .

Robust accuracy of CIFAR-10 l_2 -robust model										
metric	ϵ	DF	DAA-1	DAA-50	PGD-1	PGD-100	PGD-500	FAB-1	FAB-10	FAB-100
l_∞	$2/255$	64.1	67.2	66.3	62.6	62.6	62.6	62.7	62.6	62.6
	$4/255$	49.0	65.0	62.8	45.7	45.1	45.0	44.6	44.4	44.2
	$6/255$	36.9	64.2	60.8	33.5	32.0	31.6	27.6	26.9	26.8
	$8/255$	25.8	62.3	58.0	26.1	23.9	23.5	15.3	14.2	13.7
	$10/255$	17.6	61.9	54.8	20.4	17.7	17.3	8.8	8.1	8.0
		CW	DF	LRA	PGD-1	PGD-100	PGD-500	FAB-1	FAB-10	FAB-100
l_2	0.25	66.0	67.0	65.6	65.8	65.6	65.6	65.6	65.6	65.6
	0.5	48.2	53.8	47.8	50.2	49.6	49.2	48.4	48.2	48.0
	0.75	32.6	42.2	32.4	46.4	43.8	43.4	32.8	32.2	32.2
	1	21.6	30.0	21.6	44.8	42.2	41.4	21.8	21.6	21.0
	1.25	11.4	22.4	12.4	44.4	40.8	39.6	12.4	12.2	11.8
		SparseFool	EAD	PGD-1	PGD-50	PGD-100	FAB-1	FAB-10	FAB-100	
l_1	3		69.5	62.2	58.1	57.9	57.9	63.7	63.1	63.0
	6		61.6	45.5	44.2	43.1	42.9	49.1	47.6	46.1
	9		53.1	27.7	32.4	30.9	30.1	33.6	30.4	29.0
	12		44.4	17.9	25.0	24.3	23.1	24.0	19.8	17.8
	15		37.0	10.4	20.6	18.2	16.6	16.5	12.4	10.7

Table 5: Comparison of l_∞ -, l_2 - and l_1 -attacks on a naturally trained model on CIFAR-10. We report the accuracy in percentage of the classifier on the test set if the attack is allowed to perturb the test points of ϵ in l_p -distance. The statistics are computed on the first 1000 points on the test set for l_∞ and l_1 , on 500 points for l_2 .

Robust accuracy of CIFAR-10 plain model										
metric	ϵ	DF	DAA-1	DAA-50	PGD-1	PGD-100	PGD-500	FAB-1	FAB-10	FAB-100
l_∞	$1/255$	62.6	65.7	64.1	56.5	56.1	56.1	57.1	56.1	56.0
	$1.5/255$	49.3	63.2	60.8	40.3	38.6	38.3	39.8	38.2	37.7
	$2/255$	37.3	62.4	58.5	26.0	23.9	23.2	24.2	22.5	21.5
	$2.5/255$	26.4	61.2	56.3	17.1	14.7	14.6	14.4	12.4	12.1
	$3/255$	19.0	60.2	54.4	11.9	9.8	9.5	7.3	5.9	5.7
		CW	DF	LRA	PGD-1	PGD-100	PGD-500	FAB-1	FAB-10	FAB-100
l_2	0.1	69.4	72.2	69.0	68.4	67.6	67.6	68.6	68.6	68.4
	0.15	55.4	62.6	55.0	54.6	54.2	54.2	54.6	54.0	53.8
	0.2	43.4	51.2	43.4	45.2	44.0	43.4	43.2	42.4	42.2
	0.3	21.6	33.8	22.0	31.2	29.4	29.2	21.6	21.0	20.6
	0.4	9.4	20.8	9.8	26.8	23.8	23.0	10.0	8.2	8.0
		SparseFool	EAD	PGD-1	PGD-50	PGD-100	FAB-1	FAB-10	FAB-100	
l_1	2		72.1	54.7	54.9	53.9	53.6	55.5	52.9	50.5
	4		58.6	24.1	27.4	26.0	25.3	31.0	25.3	23.2
	6		45.6	8.9	14.7	12.3	11.6	15.7	10.4	8.3
	8		34.3	3.0	7.7	6.2	5.6	7.2	3.4	2.4
	10		27.2	0.7	4.9	3.5	2.9	3.3	1.2	0.8

Table 6: Comparison of l_∞ -, l_2 - and l_1 -attacks on an l_∞ -robust model on CIFAR-10. We report the accuracy in percentage of the classifier on the test set if the attack is allowed to perturb the test points of ϵ in l_p -distance. The statistics are computed on the first 1000 points on the test set for l_∞ and l_1 , on 500 points for l_2 .

Robust accuracy of CIFAR-10 l_∞ -robust model										
metric	ϵ	DF	DAA-1	DAA-50	PGD-1	PGD-100	PGD-500	FAB-1	FAB-10	FAB-100
l_∞	$2/255$	66.8	66.9	66.3	65.5	65.5	65.5	65.8	65.8	65.7
	$4/255$	53.2	63.8	61.4	50.2	49.3	49.2	49.5	49.1	49.0
	$6/255$	42.9	63.1	58.4	38.3	37.3	37.1	35.7	35.0	34.7
	$8/255$	32.9	61.2	56.3	31.0	29.2	28.8	24.4	23.4	23.3
	$10/255$	24.5	59.8	54.1	24.9	21.6	21.4	15.7	14.7	14.5
		CW	DF	LRA	PGD-1	PGD-100	PGD-500	FAB-1	FAB-10	FAB-100
l_2	0.25	64.6	67.0	64.4	64.4	64.4	64.4	64.8	64.4	64.4
	0.5	48.4	53.0	48.8	50.2	49.2	49.2	48.6	48.6	48.2
	0.75	33.4	41.4	33.4	44.8	43.2	42.8	33.8	33.4	33.2
	1	22.8	32.6	22.8	43.0	41.0	40.6	22.8	22.2	22.0
	1.25	12.0	24.2	13.0	41.8	40.0	38.8	12.8	12.0	11.4
		SparseFool	EAD	PGD-1	PGD-50	PGD-100	FAB-1	FAB-10	FAB-100	
l_1	5		57.8	36.8	65.5	65.5	65.5	43.8	40.2	38.6
	8.75		44.7	19.2	50.2	49.5	49.3	26.3	23.1	21.0
	12.5		34.9	7.1	38.3	38.0	37.3	14.6	10.8	8.9
	16.25		27.6	3.0	31.0	29.9	29.2	6.8	4.7	3.8
	20		20.2	0.9	24.9	22.4	21.6	4.3	1.9	1.2

Table 7: Comparison of l_∞ -, l_2 - and l_1 -attacks on a naturally trained model on Restricted ImageNet. We report the accuracy in percentage of the classifier on the test set if the attack is allowed to perturb the test points of ϵ in l_p -distance. The statistics are computed on the first 500 points of the test set.

Robust accuracy of Restricted ImageNet plain model								
metric	ϵ	DF	DAA-1	DAA-10	PGD-1	PGD-50	FAB-1	FAB-10
l_∞	$0.25/255$	76.6	74.8	74.8	74.8	74.8	78.0	76.8
	$0.5/255$	52.0	51.8	48.2	38.8	38.4	49.6	46.2
	$0.75/255$	26.8	46.0	41.0	13.2	12.8	28.0	19.8
	$1/255$	11.2	43.2	39.4	4.0	4.0	17.4	10.2
	$1.25/255$	5.0	41.2	38.2	1.2	1.2	12.4	5.4
			DF	PGD-1	PGD-50	FAB-1	FAB-10	
l_2	0.2		80.2	76.6	76.4	76.2	76.2	
	0.4		58.4	41.0	40.8	41.6	41.4	
	0.6		33.8	16.4	16.2	18.0	16.8	
	0.8		18.8	4.2	4.2	4.6	4.4	
	1		8.6	1.8	1.8	1.2	1.0	
		SparseFool	PGD-1	PGD-20	FAB-1	FAB-10		
l_1	5		88.6	83.8	83.8	79.2	76.6	
	16		80.0	51.6	51.2	47.0	40.0	
	27		70.6	23.8	23.2	27.8	19.4	
	38		65.0	8.4	8.2	14.2	8.4	
	49		55.4	3.8	3.6	9.4	3.8	

Table 8: Comparison of l_∞ -, l_2 - and l_1 -attacks on an l_∞ -robust model on Restricted ImageNet. We report the accuracy in percentage of the classifier on the test set if the attack is allowed to perturb the test points of ϵ in l_p -distance. The statistics are computed on the first 500 points of the test set.

Robust accuracy of Restricted ImageNet l_∞ -robust model								
metric	ϵ	DF	DAA-1	DAA-10	PGD-1	PGD-50	FAB-1	FAB-10
l_∞	$2/255$	75.8	75.0	75.0	75.0	75.0	75.0	74.6
	$4/255$	53.0	46.2	46.2	46.6	46.2	47.8	46.6
	$6/255$	32.4	24.6	23.8	21.0	20.4	23.6	21.6
	$8/255$	19.4	17.0	14.6	7.0	7.0	10.0	7.2
	$10/255$	10.8	12.8	11.6	1.4	1.2	3.0	1.4
			DF	PGD-1	PGD-50	FAB-1	FAB-10	
l_2	1		79.4	76.6	76.6	76.2	76.2	
	2		65.0	48.2	47.0	49.4	48.8	
	3		46.8	23.6	22.6	24.0	23.2	
	4		32.8	9.6	8.8	10.6	10.2	
	5		20.4	3.2	3.0	3.4	3.2	
			SparseFool	PGD-1	PGD-20	FAB-1	FAB-10	
l_1	15		81.8	72.4	72.4	69.4	66.8	
	25		76.4	61.6	61.2	55.0	52.6	
	40		71.4	47.2	46.6	41.6	37.2	
	60		63.2	33.0	32.6	29.4	24.4	
	100		49.2	14.0	13.6	15.8	10.8	

Table 9: Comparison of l_∞ -, l_2 - and l_1 -attacks on an l_2 -robust model on Restricted ImageNet. We report the accuracy in percentage of the classifier on the test set if the attack is allowed to perturb the test points of ϵ in l_p -distance. The statistics are computed on the first 500 points of the test set.

Robust accuracy of Restricted ImageNet l_2 -robust model								
metric	ϵ	DF	DAA-1	DAA-10	PGD-1	PGD-50	FAB-1	FAB-10
l_∞	$2/255$	74.4	73.0	73.0	73.0	73.0	73.8	73.4
	$4/255$	49.0	39.6	39.2	38.6	38.6	39.4	38.6
	$6/255$	27.4	22.6	21.0	14.4	14.2	15.4	14.2
	$8/255$	13.8	18.6	16.8	4.6	4.2	5.6	3.4
	$10/255$	6.6	15.6	13.8	0.8	0.8	2.8	0.8
			DF	PGD-1	PGD-50	FAB-1	FAB-10	
l_2	2		74.2	71.8	71.6	71.4	71.4	
	3		61.6	51.6	51.6	51.4	51.4	
	4		45.6	32.4	32.0	33.0	32.4	
	5		34.6	21.0	20.6	21.4	21.2	
	6		25.2	10.2	10.2	11.0	10.8	
			SparseFool	PGD-1	PGD-20	FAB-1	FAB-10	
l_1	50		85.4	82.6	82.2	78.6	78.4	
	100		79.6	67.4	67.0	61.6	58.8	
	150		74.4	51.2	50.8	46.2	43.2	
	200		68.6	38.0	37.8	32.4	29.2	
	250		60.0	25.8	25.0	23.8	19.8	

References

- [1] A. Athalye, N. Carlini, and D. A. Wagner. Obfuscated gradients give a false sense of security: Circumventing defenses to adversarial examples. In *ICML*, 2018.
- [2] O. Bastani, Y. Ioannou, L. Lampropoulos, D. Vytiniotis, A. Nori, and A. Criminisi. Measuring neural net robustness with constraints. In *NeurIPS*, 2016.
- [3] W. Brendel, J. Rauber, and M. Bethge. Decision-based adversarial attacks: Reliable attacks against black-box machine learning models. In *ICLR*, 2018.
- [4] T. B. Brown, D. Mané, A. Roy, M. Abadi, and J. Gilmer. Adversarial patch. In *NeurIPS 2017 Workshop on Machine Learning and Computer Security*, 2017.
- [5] N. Carlini and D. Wagner. Adversarial examples are not easily detected: Bypassing ten detection methods. In *ACM Workshop on Artificial Intelligence and Security*, 2017.
- [6] N. Carlini and D. Wagner. Towards evaluating the robustness of neural networks. In *IEEE Symposium on Security and Privacy*, 2017.
- [7] P. Chen, Y. Sharma, H. Zhang, J. Yi, and C. Hsieh. Ead: Elastic-net attacks to deep neural networks via adversarial examples. In *AAAI*, 2018.
- [8] F. Croce, J. Rauber, and M. Hein. Scaling up the randomized gradient-free adversarial attack reveals overestimation of robustness using established attacks. preprint, arXiv:1903.11359, 2019.
- [9] L. Engstrom, B. Tran, D. Tsipras, L. Schmidt, and A. Madry. A rotation and a translation suffice: Fooling CNNs with simple transformations. In *NeurIPS 2017 Workshop on Machine Learning and Computer Security*, 2017.
- [10] S. Gu and L. Rigazio. Towards deep neural network architectures robust to adversarial examples. In *ICLR Workshop*, 2015.
- [11] K. He, X. Zhang, S. Ren, and J. Sun. Deep residual learning for image recognition. In *CVPR*, pages 770–778, 2016.
- [12] M. Hein and M. Andriushchenko. Formal guarantees on the robustness of a classifier against adversarial manipulation. In *NeurIPS*, 2017.
- [13] R. Huang, B. Xu, D. Schuurmans, and C. Szepesvari. Learning with a strong adversary. In *ICLR*, 2016.
- [14] G. Katz, C. Barrett, D. Dill, K. Julian, and M. Kochenderfer. Reluplex: An efficient smt solver for verifying deep neural networks. In *CAV*, 2017.
- [15] A. Krizhevsky, V. Nair, and G. Hinton. Cifar-10 (canadian institute for advanced research).
- [16] A. Kurakin, I. J. Goodfellow, and S. Bengio. Adversarial examples in the physical world. In *ICLR Workshop*, 2017.
- [17] A. Madry, A. Makelov, L. Schmidt, D. Tsipras, and A. Valdu. Towards deep learning models resistant to adversarial attacks. In *ICLR*, 2018.
- [18] A. Modas, S. Moosavi-Dezfooli, and P. Frossard. Sparsefool: a few pixels make a big difference. In *CVPR*, 2019.
- [19] S.-M. Moosavi-Dezfooli, A. Fawzi, and P. Frossard. Deepfool: a simple and accurate method to fool deep neural networks. In *CVPR*, pages 2574–2582, 2016.
- [20] M. Mosbach, M. Andriushchenko, T. Trost, M. Hein, and D. Klakow. Logit pairing methods can fool gradient-based attacks. In *NeurIPS 2018 Workshop on Security in Machine Learning*, 2018.
- [21] N. Narodytska and S. P. Kasiviswanathan. Simple black-box adversarial perturbations for deep networks. In *CVPR 2017 Workshops*, 2016.
- [22] N. Papernot, N. Carlini, I. Goodfellow, R. Feinman, F. Faghri, A. Matyasko, K. Hambardzumyan, Y.-L. Juang, A. Kurakin, R. Sheatsley, A. Garg, and Y.-C. Lin. cleverhans v2.0.0: an adversarial machine learning library. preprint, arXiv:1610.00768, 2017.
- [23] N. Papernot, P. McDonald, X. Wu, S. Jha, and A. Swami. Distillation as a defense to adversarial perturbations against deep networks. In *IEEE Symposium on Security & Privacy*, 2016.
- [24] J. Rauber, W. Brendel, and M. Bethge. Foolbox: A python toolbox to benchmark the robustness of machine learning models. In *ICML Reliable Machine Learning in the Wild Workshop*, 2017.
- [25] J. Su, D. V. Vargas, and S. Kouichi. One pixel attack for fooling deep neural networks. preprint, arXiv:1710.08864v5, 2019.

- [26] V. Tjeng, K. Xiao, and R. Tedrake. Evaluating robustness of neural networks with mixed integer programming. In *ICLR*, 2019.
- [27] F. Tramèr and D. Boneh. Adversarial training and robustness for multiple perturbations. preprint, arXiv:1904.13000, 2019.
- [28] D. Tsipras, S. Santurkar, L. Engstrom, A. Turner, and A. Madry. Robustness may be at odds with accuracy. In *ICLR*, 2019.
- [29] E. Wong, F. R. Schmidt, and J. Z. Kolter. Wasserstein adversarial examples via projected sinkhorn iterations. preprint, arXiv:1902.07906.
- [30] H. Zhang, Y. Yu, J. Jiao, E. P. Xing, L. E. Ghaoui, and M. I. Jordan. Theoretically principled trade-off between robustness and accuracy. In *ICML*, 2019.
- [31] S. Zheng, Y. Song, T. Leung, and I. J. Goodfellow. Improving the robustness of deep neural networks via stability training. In *CVPR*, 2016.
- [32] T. Zheng, C. Chen, and K. Ren. Distributionally adversarial attack. In *AAAI*, 2019.

Table 11: We report the robust accuracy in percentage of the models and at the thresholds ϵ of Tables 7 to 9 obtained applying our attack with the final search every time an adversarial example is found (w/IS) and not only at the end (wo/IS). We use 100 iterations for l_∞ and l_2 , 300 for l_1 , 10 restarts. The statistics are computed on the first 500 points on the test set.

Robust accuracy by FAB-10 with intermediate search

Restricted ImageNet							
		plain		l_∞ -AT		l_2 -AT	
metric		wo/IS	w/IS	wo/IS	w/IS	wo/IS	w/IS
l_∞		76.8	77.2	74.6	74.6	73.4	73.2
		46.2	46.6	46.6	46.2	38.6	38.4
		19.8	21.4	21.6	21.4	14.2	14.2
		10.2	10.8	7.2	7.2	3.4	3.8
		5.4	5.8	1.4	1.4	0.8	0.8
l_2		76.2	76.2	76.2	76.2	71.4	71.4
		41.4	41.2	48.8	48.8	51.4	51.2
		16.8	16.8	23.2	22.8	32.4	32.2
		4.4	4.4	10.2	10.0	21.2	21.0
		1	1.2	3.2	3.2	10.8	10.6
l_1		76.6	77.2	66.8	67.2	78.4	78.4
		40	39.6	52.6	51.4	58.8	58.8
		19.4	19.4	37.2	36.8	43.2	42.8
		8.4	8.2	24.4	23.8	29.2	28.8
		3.8	4.0	10.8	10.8	19.8	20.4

Table 12: We report the values of ϵ used for sampling in case our FAB-attack uses random restarts.

values of ϵ used for random restarts

metric	MNIST			CIFAR-10			Restricted ImageNet		
	plain	l_∞ -AT	l_2 -AT	plain	l_∞ -AT	l_2 -AT	plain	l_∞ -AT	l_2 -AT
l_∞	0.15	0.3	0.3	0.0	0.02	0.02	0.02	0.08	0.08
l_2	2.0	2.0	2.0	0.5	4.0	4.0	5.0	5.0	5.0
l_1	40.0	40.0	40.0	10.0	10.0	10.0	100.0	250.0	250.0